




Article

Synthesis of Spin-Labelled Bergamottin: A Potent CYP3A4 Inhibitor with Antiproliferative Activity

Balázs Zoltán Zsidó¹, Mária Balog², Nikolett Erős², Miklós Poór^{3,4}, Violetta Mohos^{3,4}, Eszter Fliszár-Nyúl^{3,4}, Csaba Hetényi¹ , Masaki Nagane⁵ , Kálmán Hideg², Tamás Kálai^{2,4} and Balázs Bognár^{2,*} 

¹ Department of Pharmacology and Pharmacotherapy, University of Pécs, Medical School, Szigeti út 12, H-7624 Pécs, Hungary; zsidobalazs@pte.hu (B.Z.); csabahete@yahoo.com (C.H.)

² Institute of Organic and Medicinal Chemistry, University of Pécs, Medical School, Honvéd utca 1, H-7624 Pécs, Hungary; mariabalog@aok.pte.hu (M.B.); erosniki93@gmail.com (N.E.); kalman.hideg@aok.pte.hu (K.H.); tamaskalai@aok.pte.hu (T.K.)

³ Department of Pharmacology, University of Pécs, Faculty of Pharmacy, Szigeti út 12, H-7624 Pécs, Hungary; poor.miklos@pte.hu (M.P.); mohos.violetta@gytk.pte.hu (V.M.); eszter.nyul@aok.pte.hu (E.F.-N.)

⁴ János Szentágothai Research Center, University of Pécs, Ifjúság útja 20, H-7624 Pécs, Hungary

⁵ Department of Biochemistry, School of Veterinary Medicine, Azabu University, 1-17-71 Fuchinobe, Chuo-ku, Sagami-hara, Kanagawa 252-5201, Japan; nagane@azabu-u.ac.jp

* Correspondence: balazs.bognar@aok.pte.hu or bognar.balazs83@gmail.com; Tel.: +36-536-220

Received: 19 December 2019; Accepted: 10 January 2020; Published: 13 January 2020



Abstract: Bergamottin (BM, **1**), a component of grapefruit juice, acts as an inhibitor of some isoforms of the cytochrome P450 (CYP) enzyme, particularly CYP3A4. Herein, a new bergamottin containing a nitroxide moiety (SL-bergamottin, SL-BM, **10**) was synthesized; chemically characterized, evaluated as a potential inhibitor of the CYP2C19, CYP3A4, and CYP2C9 enzymes; and compared to BM and known inhibitors such as ketoconazole (KET) (3A4), warfarin (WAR) (2C9), and ticlopidine (TIC) (2C19). The antitumor activity of the new SL-bergamottin was also investigated. Among the compounds studied, BM showed the strongest inhibition of the CYP2C9 and 2C19 enzymes. SL-BM is a more potent inhibitor of CYP3A4 than the parent compound; this finding was also supported by docking studies, suggesting that the binding positions of BM and SL-BM to the active site of CYP3A4 are very similar, but that SL-BM had a better ΔG_{bind} value than that of BM. The nitroxide moiety markedly increased the antitumor activity of BM toward HeLa cells and marginally increased its toxicity toward a normal cell line. In conclusion, modification of the geranyl sidechain of BM can result in new CYP3A4 enzyme inhibitors with strong antitumor effects.

Keywords: bergamottin; nitroxide; CYP3A4 inhibition; anticancer activity

1. Introduction

Bergamottin (i.e., 5-geranoxypsoralen (**1**)) is a natural furanocoumarin that was originally detected in bergamot oil (*Citrus bergamia*) [1] and is mainly responsible, together with 6',7'-dihydroxybergamottin (DHB, **2**), for "grapefruit juice/drug" interactions (Figure 1). Grapefruit juice has been found to cause a marked increase in the oral bioavailability of many therapeutic agents (e.g., dihydropyridines [2], ethinylestradiol [3], midazolam [4], cyclosporine A [5], and lovastatin [6]) primarily by inhibiting the CYP3A4 enzyme. Several mechanisms have been reported regarding the CYP3A4 inhibitory effect of bergamottin such as decreased protein expression or the reversible inhibition of the enzyme [7–10].

Row et al. studied the inhibitory effects of a series of furanocoumarin analogues on the CYP3A4 enzyme. They found that the furan ring and the alkyloxy group were necessary for inhibition, and hydrophilic groups at 6',7'-positions enhanced the potency compared to the alkenyl group [11].

Although bergamottin is a less potent CYP3A4 inhibitor than DHB [12], it is a stronger inhibitor of some other CYP subfamilies such as CYP1A and 2B [13]. Bergamottin was also found to inhibit CYP2A6, 2C9, 2C19, 2D6, and 2E1 enzymes in human liver microsomes [14].

Bergamottin appeared to be a potential anticancer agent against various tumor cell lines by the regulation of several cancer-related pathways [15]. Through the inhibition of STAT3 activation, BM inhibited the proliferation of breast cancer cells and multiple myeloma [16]. BM attenuated cell migration and invasion of fibrosarcoma and lung cancer cell lines [17,18]. In combination with simvastatin, BM suppressed the TNF- α -induced anti-proliferative and pro-apoptotic processes of KBM-5 myeloid leukemia cells [19].

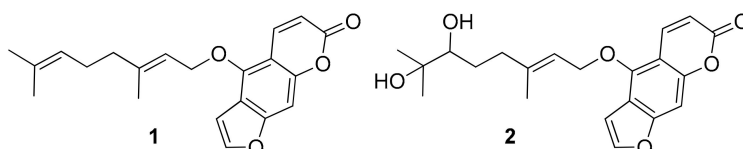


Figure 1. Chemical structures of bergamottin (1) and 6',7'-dihydroxybergamottin (2).

The unpaired electrons of stable nitroxide free radicals allow the nitroxides to take part in one-electron oxidation and reduction processes, which make nitroxides potent unnatural antioxidants [20]. As a consequence, nitroxides exert a cytoprotective action against oxidative stress induced by cytotoxic drugs or pathological processes, such as ischemia-reperfusion and inflammation [21–23]. However, some piperidine types of nitroxides also exert cytotoxic and pro-oxidant effects, particularly on cancer cells [24,25].

We have reported in several studies that the modification of biomolecules (caffeic acid phenethyl ester, resveratrol, and curcumin) with nitroxides for use as “in statu nascendi acting” antioxidants may be beneficial on their activity. For instance, better antioxidant, antiproliferative, anti-inflammatory and cell-protective compounds can be achieved by these modifications [26–31].

Herein, we report the synthesis, CYP (2C9, 2C19, and 3A4) enzyme inhibition, and the anticancer activity of a new paramagnetic bergamottin analog compared to the parent compound and known CYP inhibitors. Furthermore, CYP3A4 enzyme inhibition was also evaluated by docking studies.

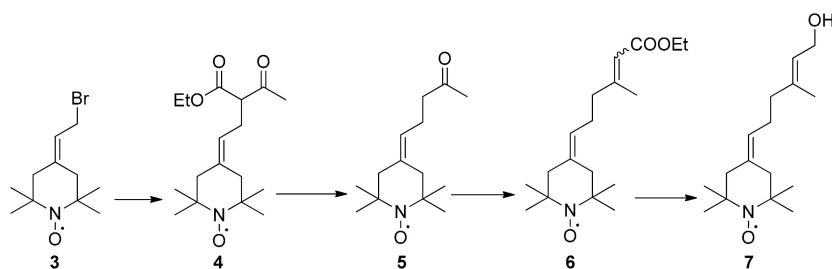
2. Results

2.1. Synthesis of Spin-Labelled Geraniol (7)

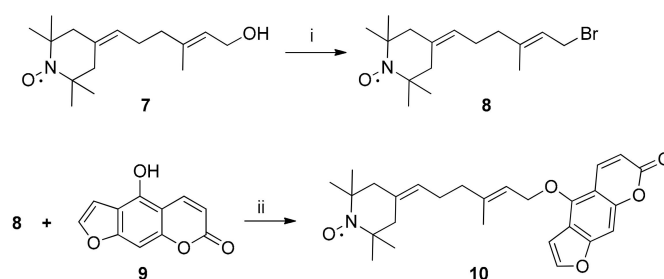
For the synthesis of nitroxide-modified geraniol (7), the first step was to alkylate the ethyl acetoacetate with paramagnetic allylic bromide (3) [32] in acetone and in the presence of K_2CO_3 at ambient temperature to obtain compound 4 with 67% yield. The ketoester was hydrolyzed with a NaOH/ethanol solution and then acidified with aq. H_2SO_4 . The elimination of CO_2 happened spontaneously to yield ketone 5, in which the Horner–Wadsworth–Emmons reaction with triethyl phosphonoacetate led to the formation of paramagnetic Z/E esters (6) at a 1:4 ratio. After purification, the reduction of E-ester 6 with sodium-bis (2-methoxyethoxy) aluminum hydride (SMEAH) in anhydrous toluene afforded E-4-(6-hydroxy-4-methyl-4-hexene-1-ylidene)-2,2,6,6-tetramethyl-piperidine-1-oxyl (7, spin-labelled geraniol) (Scheme 1).

2.2. Synthesis of Spin-Labelled Bergamottin (10)

The alkylation of 4-hydroxy-7H-furo[3,2-g]chromen-7-one (bergaptol, 9) may result in new bergamottin derivatives. To achieve a nitroxide ring motif containing bergamottin (10), paramagnetic geranyl bromide (8) was synthesized via the treatment of 7 with methanesulfonyl chloride and followed by LiBr. Bergaptol (9) was then alkylated with compound 8 in dry acetone in the presence of K_2CO_3 and catalytic amount of sodium iodide to afford SL-BM (10) (Scheme 2).



Scheme 1. Reagents and conditions: (i) potassium carbonate, ethyl acetoacetate, 18-crown-6, anhydrous acetone, 24 h reflux, 67%; (ii) 10% aqueous NaOH, ethanol, 30 min reflux followed by 24 h stirring at room temperature, then 5% H₂SO₄, 59%; (iii) NaH, anhydrous toluene, triethyl phosphonoacetate, N₂ atmosphere, 30 min reflux, 45%; (iv) SMEAH, abs. toluene, N₂ atmosphere, −30 °C, then room temperature for 30 min, 83%.



Scheme 2. Reagents and conditions: (i) dry CH₂Cl₂, triethylamine, methanesulfonyl chloride at −30 °C, then LiBr, anhydrous acetone, 40 °C, 30 min, 72%; (ii) anhydrous acetone, K₂CO₃, NaI (cat.), 40 °C, 24 h, N₂ atmosphere, 20%.

2.3. Inhibition of the CYP Enzymes by BM and SL-BM

BM proved to be a strong inhibitor of each CYP enzyme tested, while SL-BM showed considerable inhibitory effects toward the CYP2C19 and CYP3A4 enzymes (Figure 2). BM was a two-fold stronger inhibitor of CYP2C9 than the positive control warfarin (Table 1); the inhibitory effect induced by SL-BM was also statistically significant, but only a slight decrease in metabolite formation resulted (even at a four-fold concentration vs. the substrate). SL-BM was approximately two times weaker, while BM induced almost a seven-times stronger inhibitory effect toward CYP2C19 relative to the inhibitory effect of the positive control ticlopidine. Despite the fact that BM proved to be a considerably stronger inhibitor of both the CYP2C enzymes tested, SL-BM showed a significantly stronger inhibitory action toward CYP3A4 (Figure 2). BM and SL-BM were 1.7 and 8.5 times weaker inhibitors of CYP3A4 than the positive control ketoconazole (Table 1).

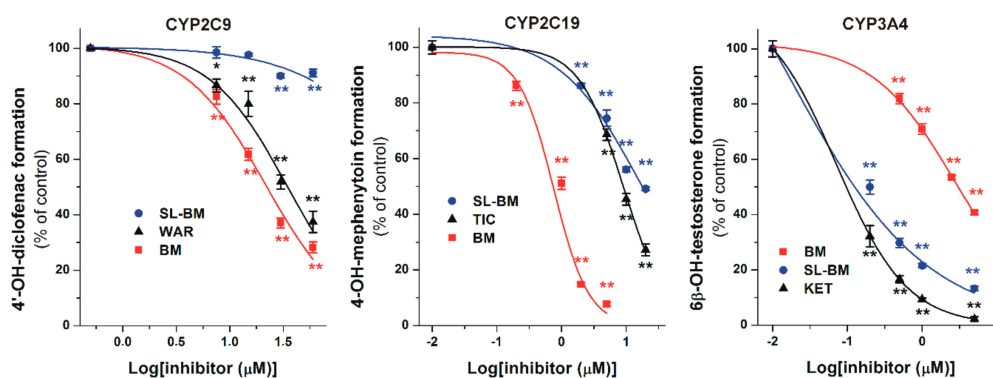


Figure 2. Concentration-dependent inhibitory effects of BM, SL-BM, and positive controls (WAR, warfarin; TIC, ticlopidine; KET, ketoconazole) towards the CYP2C9, CYP2C19, and CYP3A4 enzymes (* $p < 0.05$, ** $p < 0.01$). Data points indicate the means obtained from triplicate incubations \pm SEM.

Table 1. Inhibition of the CYP2C9, CYP2C19, and CYP3A4 enzymes by BM, SL-BM, and positive controls.

CYP2C9 Assay	Substrate Concentration (μM)	IC ₅₀ (μM) ¹	IC _{50(re)} ²	α ³
Warfarin (positive ctrl)	15	29.4	1.96	1.00
Bergamottin	15	14.7	2.94	0.50
SL-Bergamottin	15	>60.0	>4.00	-
CYP2C19 Assay	Substrate Concentration (μM)	IC ₅₀ (μM) ¹	IC _{50(re)} ²	α ³
Ticlopidine (positive ctrl)	5	7.67	1.53	1.00
Bergamottin	5	1.01	0.20	0.13
SL-Bergamottin	5	14.6	2.92	1.90
CYP3A4 Assay	Substrate Concentration (μM)	IC ₅₀ (μM) ¹	IC _{50(re)} ²	α ³
Ketoconazole (positive ctrl)	5	0.24	0.05	1.00
Bergamottin	5	2.04	0.41	8.50
SL-Bergamottin	5	0.40	0.08	1.67

¹ IC₅₀: concentration of the inhibitor which induces 50% inhibition of the metabolite formation; ² IC_{50(re)}: IC₅₀ of the inhibitor divided by the substrate concentration; ³ α : IC₅₀ of the inhibitor divided by the IC₅₀ value of the positive control.

2.4. Modeling Studies

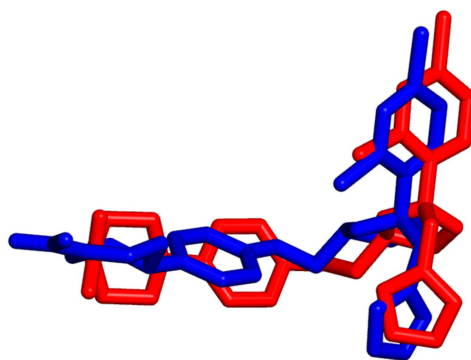
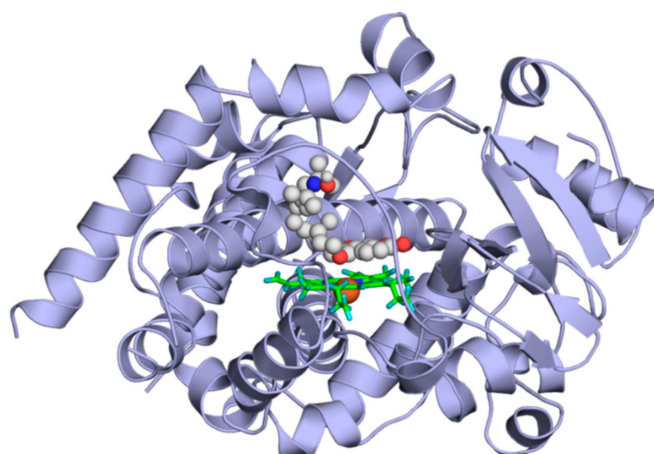
Ligands KET, BM, and **10** were docked to the binding pocket of CYP3A4, which is located above the heme ring. The docking of KET tested the applicability of the methodology for producing a close to crystallographic bound KET conformation. In the cases of BM and SL-BM, the binding modes were de novo, as described in the present study.

Binding mode of KET. According to the holo CYP3A4 crystallographic structure (Protein Data Bank (PDB) code 2v0m), KET (Table 2) is coordinated to the iron of the heme with a nitrogen of the imidazole ring, and the distance between the N atom and Fe³⁺ is 2.7 Å. Interacting amino acid residues are listed in Table 2. The heme-bound crystallographic ligand conformation of KET was used to verify the applicability of our computational docking protocol (see Methods for details) for the atomic resolution calculation of the KET binding mode. The docking of KET into the ligand-free binding pocket of the 2v0m structure was successful, and the crystallographic ligand binding mode of KET was reproduced at an RMSD value of 2.3 Å (Figure 3) in the top 2nd rank. The main interactions were reproduced. That is, the phenyl rings of F304 and KET were parallel, forming π - π interactions, and A370 formed a hydrophobic interaction with the methyl group of KET. The positively charged sidechain of R372 interacted with the partial negative charge of the oxo group of KET.

Binding modes of BM and SL-BM. To determine the binding modes of BM and SL-BM, the same docking protocol was applied as that used in the case of KET, as described in the previous paragraph. In both cases, the top 1st rank binding mode was very similar to that of KET (Figure 4). The furo[3,2-g]chromen-7-one ring was located above the heme occupying the subpockets of the imidazole ring of KET. The furan oxygen was coordinated to the heme for both ligands. The O-Fe³⁺ distances were 4.0 and 4.2 Å for compounds **10** and **1**, respectively (Figure 5). In the bound position, the furo[3,2-g]chromen-7-one ring of the ligands occupied the same subpocket and their side-chains were also in a similar position. The furo[3,2-g]chromen-7-one ring of the ligands was parallel to the heme, possibly forming π -stacking interactions, which was similar to KET (as described in the previous paragraph). Eight and seven amino acid residues were found to interact (Methods) with SL-BM and BM, respectively; of which five residues were common. Compounds **10** and **1** both interacted with CYP3A4 through H-bonds between the hydrophilic amino acid (T309) and the furan oxygen. Hydrophobic interactions occurred between the M114, F241, I301, and F304 amino acids and the methyl groups of the ligands. F304 played a role in the binding of each (KET, BM, and SL-BM) ligand (Table 2).

Table 2. Binding properties of the ligands to the CYP3A4 target. X represents the amino acid-ligand interactions.

Ligand	KET	SL-BM	BM
Rank of the docking of the ligand	2	1	1
O–Fe dist (Å)		4.2	4
N–Fe dist (Å)	3.8		
Calculated binding free energies ΔG_{bind} (kcal/mol) [33]	−9.4	−10.4	−9.2
List of interacting amino acidresidues	M114	X	X
	S119		X
	L210		X
	L211		X
	F241		X
	I301		X
	F304	X	X
	A305		X
	T309		X
	A370	X	X
	R372	X	
G481	X		

**Figure 3.** The docked (red) binding mode of KET overlaps with its crystallographic binding mode (blue), which is located above the heme ring (not shown).**Figure 4.** The binding mode of SL-BM (space-filling) as docked to the binding pocket of the CYP3A4 enzyme (light blue cartoon) above the heme ring (green sticks), where iron is represented as an orange sphere. Red spheres represent the oxygen, the blue sphere the nitrogen of SL-BM respectively.

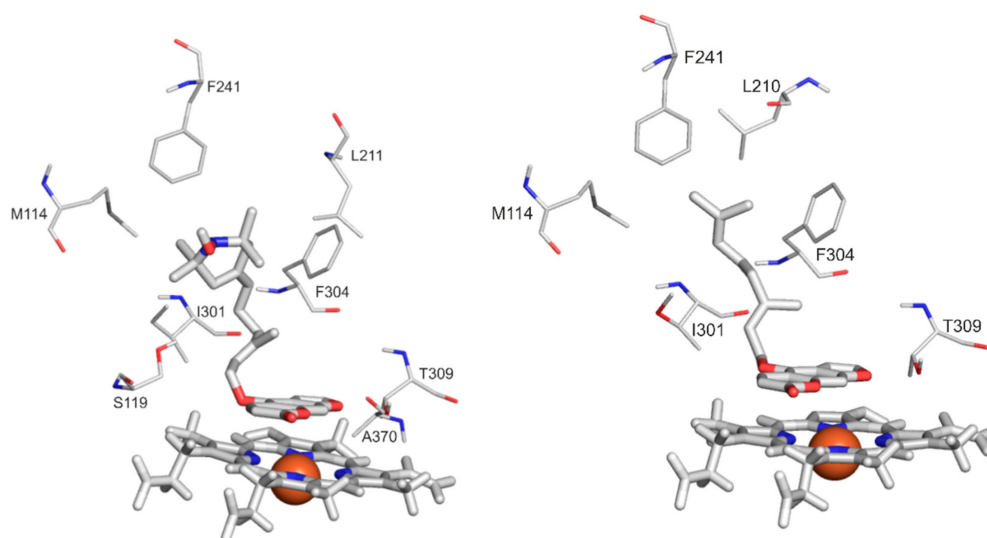


Figure 5. The close-up of the binding mode of SL-BM (left) and BM (right) (wide sticks) as docked to the binding pocket of the CYP3A4 enzyme above the heme ring (wide sticks) where iron is represented as an orange sphere. Interacting enzyme residues are labelled and shown as thin sticks.

2.5. Cytotoxicity of BM and SL-BM

The cytotoxicity of BM and SL-BM was analyzed by a WST Cell Viability & Proliferation assay performed using NIH3T3 (murine embryonic fibroblast) and HeLa (human cervix carcinoma) cells. Neither bergamottin nor SL-bergamottin showed a significant toxicity toward fibroblasts ($IC_{50} > 50 \mu M$). BM did not decrease the viability of the HeLa cells ($IC_{50} > 50 \mu M$); however, SL-BM induced a significant loss in the viability of the HeLa cell line ($IC_{50} = 17.32 \mu M$). These results demonstrate the selective toxicity of SL-BM toward cancer cells (Figure 6).

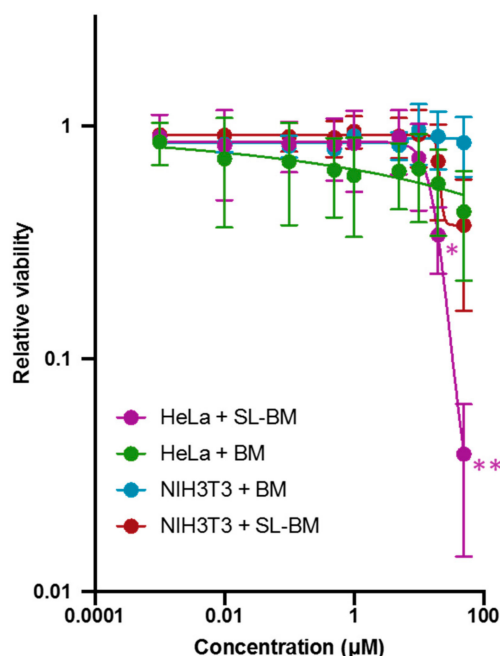


Figure 6. Concentration-dependent cytotoxic effects of BM and SL-BM on NIH3T3 fibroblasts and HeLa carcinoma cells. The cells were treated with BM or SL-BM for 24 h (* $p < 0.05$, ** $p < 0.01$). The data points represent the means \pm SD ($n = 6$).

3. Discussion

A new nitroxide moiety containing bergamottin analog (**10**) has been synthesized and evaluated for use as an inhibitor of CYP (2C9, 2C19, and 3A4) enzymes and compared to bergamottin (**1**) and known inhibitors of these enzymes. The cytotoxicity toward cancer and noncancer cell lines was also investigated.

BM induced a 50% inhibition of the metabolite formation at 0.2- and 0.4-fold concentrations vs. the substrates in the CYP2C19 and CYP3A4 assays, respectively (Table 1). The IC_{50} values of BM toward these enzymes were in the low micromolar range, which agrees well with the previously reported data [14,34–36]. Furthermore, BM proved to also be an inhibitor of CYP2C9, showing 50% inhibition of metabolite formation at approximately a three-fold concentration vs. the substrate. Previous studies also reported the significant inhibitory effect of BM on CYP2C9 enzymes [11,14,35–37]. As our results demonstrated, SL-BM only slightly inhibits CYP2C9 and is almost a 15-fold weaker inhibitor of CYP2C19 than BM (Table 1). However, SL-BM was a five-fold stronger inhibitor of CYP3A4 compared to BM, showing a strong inhibitory efficacy similar to that of the positive control ketoconazole. The enhanced inhibitory activity of SL-BM compared to that of BM was also supported by docking experiments, where the binding of SL-BM was more favorable than that of BM (ΔG_{bind} (−10.4 vs. −9.2 kcal/mol)). The difference in the inhibitory activities of SL-BM and BM may be attributed to the H-acceptor property of the nitroxide, as it was suggested by Row et al. [11].

BM and SL-BM seemed to be nontoxic to normal cells since they did not significantly decrease the viability of NIH3T3 fibroblasts in our toxicity assay. As far as we know, this is the first report about the anticancer activity of bergamottin toward HeLa cells. As shown in previous reports, although BM showed an inhibition effect on many cancer cell lines, such as HT-1080 fibrosarcoma [17], U266 multiple myeloma [18], HepG2 liver cancer, BGC-823 gastric cancer, HL-60 promyelotic leukemia [38], and A549 lung cancer cells [16], we did not observe BM to be significantly cytotoxic toward the HeLa cell line. Nevertheless, the insertion of a nitroxide moiety (**10**, IC_{50} = 17.32 μM) resulted in the cancer-specific cytotoxic activity of the parent compound (**1**, IC_{50} > 50 μM). Therefore, compound **10** may be a good starting point for the development of new CYP3A4 enzyme inhibitors with elevated anti-proliferative effects.

4. Materials and Methods

4.1. Chemistry

4.1.1. General

The mass spectra were recorded with a Thermoquest Automass Multi system (ThermoQuest, CE, Instruments, Milan, Italy) operated in EI mode (70 eV). Elemental analyses were carried out with a Fisons EA 1110 CHNS elemental analyzer (Fisons Instruments, Milan, Italy). The melting points were determined with a Boetius micro-melting point apparatus (Franz Küstner Nachf. K. G., Dresden, Germany). The ^1H NMR spectra were recorded with a Bruker Avance 3 Ascend 500 system (Bruker BioSpin Corp., Karlsruhe, Germany) operated at 500 MHz, and the ^{13}C NMR spectra were obtained at 125 MHz in CDCl_3 or DMSO-d_6 at 298 K. The “in situ” reduction of the nitroxides was achieved by the addition of five equivalents of hydrazobenzene (DPPH/radical). The IR spectra were obtained with a Bruker Alpha FT-IR instrument (Bruker Optics, Ettlingen, Germany) with an ATR support on a ZnSe plate. Flash column chromatography was performed on Merck Kieselgel 60 (0.040–0.063 mm). Qualitative TLC was carried out on commercially available plates (20 cm \times 20 cm \times 0.02 cm) coated with Merck Kieselgel (Darmstadt, Germany) GF₂₅₄. Compound **3** [32], was synthesized as previously described. All the other reagents were purchased from Sigma Aldrich (St. Louis, MO, USA), Molar Chemicals (Halásztelek, Hungary) or TCI (Tokyo, Japan). ^1H -NMR and ^{13}C -NMR spectra of new compounds are available as supporting data (see Supplementary Materials).

4.1.2. Preparation of Compounds

Ethyl 2-acetyl-4-(1-oxyl-2,2,6,6-tetramethyl-piperidin-4-ylidene)butanoate (4): Potassium carbonate (11.09 g, 80.0 mmol), ethyl acetoacetate (6.50 g, 50.0 mmol), and 18-crown-6 (10 mg) were dissolved in anhydrous acetone (30 mL), allylic bromide (3) (2.61 g, 10.0 mmol) dissolved in dry acetone (10 mL) was added dropwise, and the mixture was stirred and refluxed for 24 h. The solvent was evaporated, the residue was partitioned between H₂O (25 mL) and CH₂Cl₂ (30 mL), after separation of the phases, the water phase was extracted with further CH₂Cl₂ (2 × 20 mL). The combined organic phases were dried over MgSO₄, filtered, evaporated, and the residue was purified by column chromatography (hexane-Et₂O) to achieve compound 4 2.07 g (67%) as a red oil. R_f: 0.2 (hexane-Et₂O, 2:1), MS m/z (%): 310 (M⁺, 42), 166 (13), 135 (100), 107 (56). Anal. calcd. for C₁₇H₂₈NO₄. C 65.78; H 9.09; N 4.51, Found: C 65.55, H 9.36, N 4.42. IR (neat): $\bar{\nu}$ = 1738, 1714 cm⁻¹. ¹H NMR (500 MHz, CDCl₃ + (PhNH)₂): δ = 5.21 (t, 1H, J = 7.3 Hz), 4.26 (q, 2H, J = 7.1 Hz), 3.53 (t, 1H, J = 7.5 Hz), 2.67 (dt, 2H, J = 7.3, 2.1 Hz), 2.29 (s, 3H), 2.23 (s, 2H), 2.12 (s, 2H), 1.33 (t, 3H, J = 7.1 Hz), 1.20, 1.17 (2s, 12H). ¹³C NMR (125 MHz, CDCl₃ + (PhNH)₂): δ = 202.7, 169.5, 135.5, 121.1, 61.5, 60.2, 59.9, 49.5, 41.6, 29.2, 26.4, 14.2.

5-(1-Oxyl-2,2,6,6-tetramethylpiperidin-4-ylidene)pentan-2-one (5): To the ethanolic (20 mL) solution of ketoester (4) (1.55 g, 5.0 mmol), 10% aqueous NaOH (20 mL) was added, and the mixture was refluxed for 30 min. After additional 24 h stirring at room temperature, the solvent was evaporated off and the residue was acidified with 5% H₂SO₄ and extracted with EtOAc (3 × 20 mL). The combined organic phases were dried (MgSO₄), filtered, evaporated, and purified by flash column chromatography (hexane-Et₂O) to yield compound 5 as a red oil, 702 mg (59%); R_f: 0.23 (hexane-Et₂O, 2:1). MS (EI): m/z (%) = 238 (M⁺, 41), 224 (100), 180 (16), 166 (60), 43 (100). Anal. calcd. for C₁₄H₂₄NO₂: C, 70.55; H, 10.15; N, 5.88. Found: C, 70.39; H, 10.21; N, 5.77. IR (neat): $\bar{\nu}$ = 1714, 1633 cm⁻¹. ¹H NMR (500 MHz, CDCl₃ + (PhNH)₂): δ = 5.23 (t, 1H, J = 7.2 Hz), 2.50 (t, 2H, J = 7.5 Hz), 2.35 (q, 2H, J = 7.4 Hz), 2.20 (s, 2H), 2.16 (s, 3H), 2.11 (s, 2H), 1.19, 1.17 (2s, 12H). ¹³C NMR (125 MHz, CDCl₃ + (PhNH)₂): δ = 208.4, 133.4, 124.0, 60.3, 60.2, 49.4, 43.9, 41.6, 30.0, 22.0.

(E)-Ethyl 6-(1-oxyl-2,2,6,6-tetramethylpiperidin-4-ylidene)-3-methylhex-2-enoate (6): To a stirred suspension of NaH (96 mg, 4.0 mmol) in dry toluene (15 mL), triethyl phosphonoacetate (1.12 g, 5.0 mmol) was added at 0 °C under a N₂ atmosphere. After stirring for 10 min, 5 ketone (720 mg, 3.0 mmol) was added, and the mixture was stirred and refluxed for another 30 min. After cooling to room temperature, brine (20 cm³) and ether (20 cm³) were added, the organic phase was separated, and the aqueous phase was washed with ether (2 × 20 cm³). Then, the combined organic phase was dried (MgSO₄), filtered and evaporated, and the residue was purified by flash column chromatography (hexane-Et₂O) to yield 315 mg (34%) of compound 6 as a reddish-brown oil. R_f: 0.40 (hexane-Et₂O, 2:1); MS m/z (%) 308 (M⁺, 38), 278 (6), 166 (11), 74 (100). Anal. calcd. for C₁₈H₃₀NO₃: C, 70.09; H, 9.80; N, 4.54. Found: C, 70.19; H, 9.91; N, 4.60. IR (neat): $\bar{\nu}$ = 1713, 1648 cm⁻¹. ¹H NMR (500 MHz, CDCl₃ + (PhNH)₂): δ = 5.78 (s, 1H), 5.25 (t, 1H, J = 6.3 Hz), 4.24 (q, 2H, J = 7.1 Hz), 2.30–2.24 (m, 5H), 2.21 (s, 2H), 2.14 (s, 2H), 1.36 (t, 3H, J = 7.1 Hz), 1.21 (s, 6H), 1.19 (s, 6H). ¹³C NMR (125 MHz, CDCl₃ + (PhNH)₂): δ = 166.8, 159.3, 133.2, 124.4, 116.0, 60.3, 60.2, 59.5, 49.5, 41.7, 41.2, 25.7, 18.9, 14.4.

(E)-4-(6-hydroxy-4-methylhex-4-en-1-ylidene)-2,2,6,6-tetramethylpiperidin-1-yloxy (7): To a stirred solution of ester (6) (716 mg, 2.0 mmol) in abs. toluene (20 mL), SMEAH (1.21 g, 6.0 mmol) dissolved in toluene (10 mL) was added dropwise under N₂ at –30 °C. Then, the mixture temperature was allowed to rise to room temperature, and the reaction was stirred for a further 30 min. After completion of the reaction, the solution was added in portions to the mixture of 10 % NaOH (25 mL) and crushed ice (50 g). The phases were separated, and the aqueous phase was extracted with a mixture of THF/Et₂O (1:4) (3 × 20 mL). The combined organic phases were dried (MgSO₄), filtered, and evaporated. The title compound (7) was obtained after column chromatography (hexane-EtOAc) as a red oil (440 mg, 83%). R_f: 0.23 (hexane/EtOAc, 2:1), MS m/z (%) 266 (M⁺, 43), 95 (51), 74 (100), Anal. calcd. for C₁₆H₂₈NO₂: C, 72.14; H, 10.59; N, 5.26. Found: C, 72.31; H, 10.51; N, 5.37. IR (neat): $\bar{\nu}$ = 3412, 1670, 1098 cm⁻¹. ¹H NMR (500 MHz, CDCl₃ + (PhNH)₂): δ = 5.48 (dt, 1H, J = 6.9, 1.2 Hz), 5.26 (t, 1H, J = 7.0 Hz), 4.21 (d,

2H, $J = 6.8$ Hz), 2.23–2.19 (m, 4H), 2.14–2.10 (m, 4H), 1.73 (s, 3H), 1.19 (s, 6H), 1.17 (s, 6H). ^{13}C NMR (125 MHz, $\text{CDCl}_3 + (\text{PhNH})_2$): $\delta = 139.2, 132.3, 125.3, 123.7, 60.3, 60.2, 59.4, 49.5, 41.6, 39.8, 25.9, 16.3$.

(E)-4-(6-bromo-4-methylhex-4-en-1-ylidene)-2,2,6,6-tetramethylpiperidin-1-yloxy (8): To the stirred solution of compound 7 (532 mg, 2.0 mmol) and triethylamine (222 mg, 2.2 mmol) in dry CH_2Cl_2 (20 mL), after cooling to -30 °C, methanesulfonyl chloride (249.3 g, 2.2 mmol) was added dropwise. After the mixture temperature increased to room temperature, brine (20 mL) was added, the phases were separated, and the aqueous phase was extracted with CH_2Cl_2 (3×20 mL). The combined organic phases were dried over MgSO_4 , filtered, and evaporated. The residue was dissolved in anhydrous acetone (30 mL), to which LiBr (522 mg, 6.0 mmol) was then added, and the mixture was stirred at 40 °C for 30 min. Water (20 mL) and Et_2O (15 mL) were added, and after separation, the water phase was extracted with further Et_2O (2×20 mL). The combined organic phases were dried over MgSO_4 , filtered, and evaporated to achieve paramagnetic geranyl bromide (8) as a reddish-brown oil with a 72% (410 mg) yield. MS m/z (%) 284/286 (M^+ , 5/2), 248 (6), 109 (13), 107 (21), 95 (40), 74 (100). NMR measurements cannot be performed without the loss of the bromide function in the presence of hydrazobenzene.

(E)-4-((6-(1-hydroxy-2,2,6,6-tetramethylpiperidin-4-ylidene)-3-methylhex-2-en-1-yl)oxy)-7H-furo[3,2-g]chromen-7-one (10): Bergaptol (9) (202 mg, 1.0 mmol) was dissolved in anhydrous acetone (10 mL), K_2CO_3 (276 mg, 2.0 mmol), NaI (19.5 mg, 0.13 mmol), and bromide 8 (427 mg, 1.5 mmol) were added and the mixture was stirred at 40 °C for 24 h under a N_2 atmosphere. After cooling to room temperature, brine (20 mL) and CH_2Cl_2 (20 mL) were added, the organic phase was separated, and the aqueous phase was washed with CH_2Cl_2 (2×20 mL). Then, the combined organic phase was dried (MgSO_4), filtered, evaporated, and the residue was purified by flash column chromatography (hexane-EtOAc) to yield the title compound 10 as red crystals, 90 mg (20 %). M.p.: 51–53 °C. R_f : 0.43 (hexane-EtOAc, 2:1). MS m/z (%) 450 (M^+ , 3), 435 (3), 420 (5), 202 (25), 98 (66), 74 (100) Anal. calcd. for $\text{C}_{27}\text{H}_{32}\text{NO}_5$: C 71.98; H 7.16; N 3.11. Found: C, 72.11; H, 7.20; N, 3.17. IR (neat): $\bar{\nu} = 1725, 1623, 1332$ cm^{-1} . ^1H NMR (500 MHz, $\text{CDCl}_3 + (\text{PhNH})_2$): $\delta = 8.19$ (d, 1H, $J = 9.8$ Hz), 7.60 (d, 1H, $J = 2.3$ Hz), 7.20 (s, 1H), 6.96 (d, 1H, $J = 2.3$), 6.32 (d, 1H, $J = 9.8$ Hz), 5.95 (dt, 1H, $J = 6.8, 1.0$ Hz), 5.23 (t, 1H, $J = 6.8$ Hz), 4.97 (d, 2H, $J = 6.8$ Hz), 2.24–2.18 (m, 6H), 2.10 (s, 2H), 1.75 (s, 3H), 1.18 (s, 6H), 1.16 (s, 6H). ^{13}C NMR (125 MHz, $\text{CDCl}_3 + (\text{PhNH})_2$): $\delta = 161.2, 158.1, 148.9, 144.9, 142.6, 139.5, 132.7, 124.8, 119.2, 114.2, 112.6, 107.5, 105.0, 94.2, 69.7, 60.3, 60.2, 49.5, 41.7, 39.8, 25.7, 16.7$.

4.2. CYP Inhibition Assays

4.2.1. Reagents

Testosterone, 6 β -hydroxytestosterone, ketoconazole, racemic warfarin, ticlopidine hydrochloride, CypExpressTM 2C9 kit, CypExpressTM 2C19 kit, and CypExpressTM 3A4 kit were purchased from Sigma-Aldrich (St. Louis, MO, USA). Diclofenac, 4'-hydroxydiclofenac, S-mephenytoin, and 4-hydroxymephenytoin were obtained from Carbosynth (Compton, Berkshire, UK).

4.2.2. CYP Assays

Stock solutions of BM, SL-BM, and positive controls (each 5000 μM) were prepared in dimethyl sulfoxide (Fluka) and stored at -20 °C. The inhibitory effects of BM and SL-BM on the CYP2C9, 2C19, and 3A4 enzymes were examined using CypExpressTM assay kits by employing diclofenac, S-mephenytoin, and testosterone substrates, respectively. During these assays, racemic warfarin (2C9), ticlopidine (2C19), and ketoconazole (3A4) were applied as positive controls. The CYP2C9, 2C19, and 3A4 assays were performed as described in our previous studies [39–42].

The substrates and products were analyzed using the HPLC system comprising a pump (Waters 510; Milford, MA, USA), an injector (Rheodyne 7125) with a 20 μL sample loop, and a UV detector (Waters 486). The data were evaluated by employing Millennium Chromatographic Manager software (Waters). HPLC analyses of diclofenac and 4'-hydroxydiclofenac (CYP2C9 assay) [39,40],

S-mephenytoin, and 4-hydroxymephenytoin [42] as well as testosterone and 6 β -hydroxytestosterone (CYP3A4 assay) [41] were performed as described previously.

Data were derived from at least three independent experiments and represented as the mean \pm the standard error of the mean (SEM) values. The statistical significance ($p < 0.05$ and $p < 0.01$) was established by employing a one-way ANOVA test (IBS SPSS Statistics, v. 21; Armonk, NY, USA). The metabolite formation (% of control) was plotted as a function of the logarithmic concentrations, and then the IC₅₀ values were determined using GraphPad Prism 8 software (San Diego, CA, USA).

4.3. Modeling Studies

4.3.1. Ligand Preparation

The raw ligand structures of ketoconazole, bergamottin (BM, **1**), and SL-BM (**10**) were built in Maestro [43] and energy-minimized with a quantum chemistry program package, MOPAC [33], with PM7 parametrization [44]. Force calculations were also performed using MOPAC, in which the gradient norm was set to 0.001, and the force constant matrices were positive and definite. Gasteiger–Marsilli partial charges were assigned in AutoDock Tools [45]. Flexibility was allowed on the ligand at all active torsions. These prepared structures were used for docking.

4.3.2. Target Preparation

Similar to a previous study [46], the holo structure of CYP3A4 in the complex with ketoconazole was used as a target. The atomic coordinates of the complex were obtained from the Protein Data Bank (PDB) with PDB code 2v0m. The bound ketoconazole molecules were removed prior to the docking calculations, and chain A was processed further as a target. The atomic partial charges of the heme were adopted as the ferric penta coordinate high-spin charge model from reference [47]. The rest of the target molecule was equipped with polar hydrogen atoms and Gasteiger–Marsilli partial charges in AutoDock Tools.

4.3.3. Docking

All the ligand structures were docked to the active site of CYP3A4 using AutoDock 4.2.6 [45]. The number of grid points was set to 90 \times 90 \times 90 using a 0.375 Å grid spacing. The Lamarckian genetic algorithm was used for the global search, and the flexibility of all active torsions was allowed on the ligand. Ten docking runs were performed, and the resulting ligand conformations were ranked by their free binding energy values. Representative docked ligand conformations were used for the subsequent evaluations, and a collection of interacting target amino acid residues with a 3.5 Å cut-off distance were calculated for heavy atoms. The root-mean-squared deviation (RMSD) values were calculated between the crystallographic and representative ligand conformations.

4.4. Cell Viability Assays

Murine embryonic fibroblast NIH3T3 cells were maintained in DMEM (Cat No. 043-30085, Wako Pure Chemical, Osaka, Japan) supplemented with 10% newborn calf serum (NBCS) at 37 °C and 5% CO₂. Human cervix carcinoma HeLa cells were maintained in DMEM supplemented with 10% fetal bovine serum at 37 °C and 5% CO₂. To determine the toxicity of BM and SL-BM, the WST-1 cell viability assay was employed as described previously [26]. The cells (NIH3T3: 2000 per well; HeLa: 5000 per well) were seeded into all the wells of 96-well plates. After 24 h, the medium was replaced, and the cells were treated with the test compounds for 24 h. Then, the cells were incubated with a WST-1 solution (3.6 μ g/ μ L WST-1, 70 ng/ μ L 1-methoxy phenazine methosulfate in 20 mM 4-(2-hydroxyethyl)-1-piperazineethanesulfonic acid–KOH (pH 7.4); Dojindo, Kumamoto, Japan) for 1 h at 37 °C, and the absorbance of each well was recorded at 440 nm using a Multiskan FC microplate reader (Thermo Fisher Scientific). The IC₅₀ values and statistical significance were calculated using GraphPad Prism 8 software (San Diego, CA, USA).

Supplementary Materials: Supplementary materials can be found at <http://www.mdpi.com/1422-0067/21/2/508/s1>.

Author Contributions: M.P., E.F.-N., and V.M. performed the CYP enzyme assays and carried out the corresponding HPLC analyses and evaluations. B.Z.Z. and C.H. carried out the docking studies. M.N. tested the cytotoxic activity of the compounds. M.B., N.E., K.H., T.K., and B.B. designed, synthesized, and chemically characterized the new compounds. All authors have read and agreed to the published version of the manuscript.

Funding: This work was supported by the Hungarian National Research, Development and Innovation Office (FK124331: B.B K123836: B.Z. and C.H.). The research was financed by the Higher Education Excellence Programme of the Ministry for Innovation and Technology in Hungary (TUDFO/47138/2019-ITM), within the programme of University of Pécs. C.H.'s work was supported by a grant co-financed by Hungary and the European Union (EFOP-3.6.2-16-2017-00008).

Acknowledgments: This paper was supported by the János Bolyai Research Scholarship of the Hungarian Academy of Sciences. We acknowledge the computer time granted from the Governmental Information Technology Development Agency, Hungary.

Conflicts of Interest: The authors declare no conflicts of interest.

References

1. Späth, E.; Kainrath, P. Über bergamottin und über die auffindung von limettin im bergamottöl (XXXIV. mitteil. über natürliche cumarine). *Eur. J. Inorg. Chem.* **1937**, *70*, 2272–2276. [[CrossRef](#)]
2. Bailey, D.G.; Spence, J.D.; Munoz, C.; Arnold, J.M.O. Interaction of citrus juices with felodipine and nifedipine. *Lancet* **1991**, *337*, 268–269. [[CrossRef](#)]
3. Weber, A.; Jager, R.; Borner, A.; Klinger, G.; Volland, R.; Mathey, K.; Balogh, A. Can grapefruit juice influence ethinylestradiol bioavailability. *Contraception* **1996**, *53*, 41–47. [[CrossRef](#)]
4. Kuferschmidt, H.H.; Ha, H.R.; Ziegler, W.H.; Meier, P.J.; Krähenbühl, S. Interaction between grapefruit juice and midazolam in humans. *Clin. Pharmacol. Ther.* **1995**, *58*, 20–28. [[CrossRef](#)]
5. Ducharme, M.P.; Warbasse, L.H.; Edwards, D. Disposition of intravenous and oral cyclosporine after administration with grapefruit juice. *J. Clin. Pharmacol. Ther.* **1995**, *40*, 485–491. [[CrossRef](#)]
6. Kantola, T.; Kivisto, K.T.; Neuvonen, P.J. Grapefruit juice greatly increases serum concentrations of lovastatin and lovastatin acid. *Clin. Pharmacol. Ther.* **1998**, *63*, 397–402. [[CrossRef](#)]
7. Lown, K.S.; Bailey, D.G.; Fontana, R.J.; Janardan, S.K.; Adair, C.H.; Fortlage, L.A.; Brown, M.B.; Gao, W.; Watkins, P.B. Grapefruit juice increases felodipine oral availability in humans by decreasing intestinal CYP3A protein expression. *J. Clin. Invest.* **1997**, *99*, 2545–2553. [[CrossRef](#)]
8. Bailey, D.G.; Arnold, J.; Arnold, O.; Spence, J.D. Grapefruit juice-drug interactions. *Br. J. Clin. Pharmacol.* **1998**, *46*, 101–110. [[CrossRef](#)]
9. Schmiedlin-Ren, P.; Edwards, D.J.; Fitzsimmons, M.E.; He, K.; Lown, K.S.; Woster, P.M.; Rahman, A.; Thummel, K.E.; Fisher, J.M.; Hollenberg, P.F.; et al. Mechanisms of enhanced oral availability of CYP3A4 substrates by grapefruit constituents. Decreased enterocyte CYP3A4 concentration and mechanism-based inactivation by furanocoumarins. *Drug. Metab. Dispos.* **1997**, *25*, 1228–1233.
10. Guo, L.Q.; Fukuda, K.; Ohta, T.; Yamazoe, Y. Role of furanocoumarin derivatives on grapefruit juice-mediated inhibition of human CYP3A activity. *Drug. Metab. Dispos.* **2000**, *28*, 766–771. [[PubMed](#)]
11. Row, E.C.; Brow, S.A.; Stachulski, A.V.; Lennard, M.S. Design, synthesis and evaluation of furanocoumarin monomers as inhibitors of CYP3A4. *Org. Biomol. Chem.* **2006**, *4*, 1604–1610. [[CrossRef](#)] [[PubMed](#)]
12. Ohnishi, A.; Matsuo, H.; Yamada, S.; Takanaga, H.; Morimoto, S.; Shoyama, Y.; Ohtani, H.; Sawada, Y. Effect of furanocoumarin derivatives in grapefruit juice on the uptake of vinblastine by Caco-2 cells and on the activity of cytochrome P450 3A4. *Br. J. Pharmacol.* **2000**, *130*, 1369–1377. [[CrossRef](#)]
13. Olguín-Reyes, S.; Camacho-Carranza, R.; Hernández-Ojeda, S.; Elinos-Baez, M.; Espinosa-Aguirre, J.J. Bergamottin is a competitive inhibitor of CYP1A1 and is antimutagenic in the Ames test. *Food Chem. Toxicol.* **2012**, *50*, 3094–3099. [[CrossRef](#)] [[PubMed](#)]
14. He, K.; Iyer, K.R.; Hayes, R.N.; Sinz, M.W.; Woolf, T.F.; Hollenberg, P.F. Inactivation of cytochrome P450 3A4 by bergamottin, a component of grapefruit juice. *Chem. Res. Toxicol.* **1998**, *11*, 252–259. [[CrossRef](#)] [[PubMed](#)]
15. Jeong-Hyeon, K.; Frank, A.; Gautam, S.; Kwang, S.A. Pharmacological Utilization of Bergamottin, Derived from Grapefruits, in Cancer Prevention and Therapy. *Int. J. Mol. Sci.* **2018**, *19*, 4048–4060. [[CrossRef](#)]

16. Kim, S.M.; Lee, J.H.; Sethi, G.; Kim, C.; Baek, S.H.; Nam, D.; Chung, W.S.; Kim, S.H.; Shim, B.S.; Ahn, K.S. Bergamottin, a natural furanocoumarin obtained from grapefruit juice induces chemosensitization and apoptosis through the inhibition of STAT3 signaling pathway in tumor cells. *Cancer Lett.* **2014**, *354*, 153–163. [[CrossRef](#)]
17. Hwang, Y.P.; Yun, H.J.; Choi, J.H.; Kang, K.W.; Jeong, H.G. Suppression of phorbol-12-myristate-13-acetate-induced tumor cell invasion by bergamottin via the inhibition of protein kinase C δ /p38 mitogen-activated protein kinase and JNK/nuclear factor- κ B-dependent matrix metalloproteinase-9 expression. *Mol. Nutr. Food Res.* **2010**, *54*, 977–990. [[CrossRef](#)]
18. Wu, H.J.; Wu, H.B.; Zhao, Y.Q.; Chen, L.J.; Zou, H.Z. Bergamottin isolated from Citrus bergamia exerts in vitro and in vivo antitumor activity in lung adenocarcinoma through the induction of apoptosis, cell cycle arrest, mitochondrial membrane potential loss and inhibition of cell migration and invasion. *Oncol. Rep.* **2016**, *36*, 324–332. [[CrossRef](#)]
19. Kim, S.M.; Lee, E.J.; Lee, J.H.; Yang, W.M.; Nam, D.; Lee, J.H.; Lee, S.G.; Um, J.Y.; Shim, B.S.; Ahn, K.S. Simvastatin in combination with bergamottin potentiates TNF-induced apoptosis through modulation of NF-kappaB signalling pathway in human chronic myelogenous leukaemia. *Pharm. Boil.* **2016**, *54*, 2050–2060. [[CrossRef](#)]
20. Krishna, M.C.; DeGraff, W.; Hankovszky, H.O.; Sár, P.C.; Kálai, T.; Jeko, J.; Russo, A.; Mitchell, J.B.; Hideg, K. Studies of Structure–Activity Relationship of Nitroxide Free Radicals and Their Precursors as Modifiers Against Oxidative Damage. *J. Med. Chem.* **1998**, *41*, 3477–3492. [[CrossRef](#)]
21. Monti, E.; Cova, D.; Guido, E.; Morelli, R.; Oliva, C. Protective effect of the nitroxide tempol against the cardiotoxicity of adriamycin. *Free Radic. Biol. Med.* **1996**, *21*, 463–470. [[CrossRef](#)]
22. Howard, B.J.; Yatin, S.; Hensley, K.; Allen, K.L.; Kelly, J.P.; Carney, J.; Butterfield, D.A. Prevention of Hyperoxia-Induced Alterations in Synaptosomal Membrane-Associated Proteins by N-tert-Butyl- α -Phenylnitron and 4-Hydroxy-2,2,6,6-Tetramethylpiperidin-1-oxyl (Tempol). *J. Neurochem.* **1996**, *67*, 2045–2050. [[CrossRef](#)] [[PubMed](#)]
23. Deres, P.; Halmosi, R.; Tóth, A.; Kovács, K.; Pálfi, A.; Habon, T.; Czopf, L.; Kálai, T.; Hideg, K.; Sümegi, B.; et al. Prevention of doxorubicin-induced acute cardiotoxicity by an experimental antioxidant compound. *J. Cardiovasc. Pharmacol.* **2005**, *45*, 36–43. [[CrossRef](#)] [[PubMed](#)]
24. Suy, S.; Mitchell, J.B.; Ehleiter, D.; Haimovitz-Friedman, A.; Kasid, U. Nitroxides Tempol and Tempo Induce Divergent Signal Transduction Pathways in MDA-MB 231 Breast Cancer Cells. *J. Biol. Chem.* **1998**, *273*, 17871–17878. [[CrossRef](#)]
25. Suy, S.; Mitchell, J.B.; Samuni, A.; Mueller, S.; Kasid, U. Nitroxide tempo, a small molecule, induces apoptosis in prostate carcinoma cells and suppresses tumor growth in athymic mice. *Cancer* **2005**, *103*, 1302–1313. [[CrossRef](#)]
26. Nagane, M.; Yamashita, T.; Vörös, P.; Kálai, T.; Hideg, K.; Bognár, B. Synthesis and evaluation of paramagnetic caffeic acid phenethyl ester (CAPE) analogs. *Monatsh. Chem.* **2019**, *150*, 1513–1522. [[CrossRef](#)]
27. Kálai, T.; Borza, E.; Antus, C.; Radnai, B.; Gulyás-Fekete, G.; Fehér, A.; Sümegi, B.; Hideg, K. Synthesis and study of new paramagnetic resveratrol analogues. *Bioorg. Med. Chem.* **2011**, *19*, 7311–7317. [[CrossRef](#)]
28. Dayton, A.; Selvendiran, K.; Meduru, S.; Khan, M.; Kuppusamy, M.L.; Naidu, S.; Kálai, T.; Hideg, K.; Kuppusamy, P. Amelioration of Doxorubicin-Induced Cardiotoxicity by an Anticancer-Antioxidant Dual-Function Compound HO-3867. *J. Pharm. Exp. Ther.* **2011**, *339*, 350–357. [[CrossRef](#)]
29. Kálai, T.; Kuppusamy, M.L.; Balog, M.; Selvendiran, K.; Rivera, B.K.; Kuppusamy, P.; Hideg, K. Synthesis of N-Substituted 3,5-Bis(arylidene)-4-piperidones with High Antitumor and Antioxidant Activity. *J. Med. Chem.* **2011**, *54*, 5414–5421. [[CrossRef](#)]
30. Ravi, Y.; Selvendiran, K.; Naidu, S.; Meduru, S.; Citro, L.A.; Bognár, B.; Khan, M.; Kálai, T.; Hideg, K.; Kuppusamy, P.; et al. Pulmonary Hypertension Secondary to Left-Heart Failure Involves Peroxynitrite-Induced Downregulation of PTEN in the Lung. *Hypertension* **2013**, *61*, 593–601. [[CrossRef](#)]
31. Bognár, B.; Kuppusamy, M.L.; Madan, E.; Kálai, T.; Balog, M.; Jekő, J.; Kuppusamy, P.; Hideg, K. Synthesis and Biological Evaluation of Curcumin-Nitroxide-Based Molecular Hybrids as Antioxidant and Anti-Proliferative Agents. *Med. Chem.* **2017**, *13*, 761–772. [[CrossRef](#)] [[PubMed](#)]
32. Stewart, J.J.P. *MOPAC2009, 2009*; Steward Computational Chemistry: Colorado Springs, CO, USA, 2008.
33. Stewart, J.J.P. Optimization of parameters for semiempirical methods VI: More modifications to the NDDO approximations and re-optimization of parameters. *J. Mol. Model.* **2013**, *19*, 1–32. [[CrossRef](#)] [[PubMed](#)]

34. Girenavar, B.; Poulouse, S.M.; Jayaprakasha, G.K.; Bhat, N.G.; Patil, B.S. Furocoumarins from grapefruit juice and their effect on human CYP 3A4 and CYP 1B1 isoenzymes. *Bioorg. Med. Chem.* **2006**, *14*, 2606–2612. [[CrossRef](#)] [[PubMed](#)]
35. Tassaneeyakul, W.; Guo, L.Q.; Fukuda, K.; Ohta, T.; Yamazoe, Y. Inhibition selectivity of grapefruit juice components on human cytochromes P450. *Arch. Biochem. Biophys.* **2000**, *378*, 356–363. [[CrossRef](#)] [[PubMed](#)]
36. Kimura, Y.; Ito, H.; Ohnishi, R.; Hatano, T. Inhibitory effects of polyphenols on human cytochrome P450 3A4 and 2C9 activity. *Food Chem. Toxicol.* **2010**, *48*, 429–435. [[CrossRef](#)]
37. Girenavar, B.; Jayaprakasha, G.K.; Patil, B.S. Potent inhibition of human cytochrome P450 3A4, 2D6, and 2C9 isoenzymes by grapefruit juice and its furocoumarins. *J. Food. Sci.* **2007**, *72*, 417–421. [[CrossRef](#)]
38. Liu, Y.; Ren, C.; Cao, Y.; Wang, Y.; Duan, W.; Xie, L.; Sun, C.; Li, X. Characterization and Purification of Bergamottin from Citrus grandis (L.) Osbeck cv. Yongjiazaoxiangyou and Its Antiproliferative Activity and Effect on Glucose Consumption in HepG2 cells. *Molecules* **2017**, *22*, 1227–1239. [[CrossRef](#)]
39. Poór, M.; Boda, G.; Needs, P.W.; Kroon, P.A.; Lemli, B.; Bencsik, T. Interaction of quercetin and its metabolites with warfarin: Displacement of warfarin from serum albumin and inhibition of CYP2C9 enzyme. *Biomed. Pharmacother.* **2017**, *88*, 574–581. [[CrossRef](#)]
40. Poór, M.; Boda, G.; Mohos, V.; Kuzma, M.; Bálint, M.; Hetényi, C.; Bencsik, T. Pharmacokinetic interaction of diosmetin and silibinin with other drugs: Inhibition of CYP2C9-mediated biotransformation and displacement from serum albumin. *Biomed. Pharmacother.* **2018**, *102*, 912–921. [[CrossRef](#)]
41. Mohos, V.; Bencsik, T.; Boda, G.; Fliszár-Nyúl, E.; Lemli, B.; Kunsági-Máté, S.; Poór, M. Interactions of casticin, ipriflavone, and resveratrol with serum albumin and their inhibitory effects on CYP2C9 and CYP3A4 enzymes. *Biomed. Pharmacother.* **2018**, *107*, 777–784. [[CrossRef](#)]
42. Fliszár-Nyúl, E.; Mohos, V.; Bencsik, T.; Lemli, B.; Kunsági-Máté, S.; Poór, M. Interactions of 7,8-Dihydroxyflavone with Serum Albumin as well as with CYP2C9, CYP2C19, CYP3A4, and Xanthine Oxidase Biotransformation Enzymes. *Biomolecules* **2019**, *9*, 655–667. [[CrossRef](#)] [[PubMed](#)]
43. LLC. *Schrödinger Release 2019-3: Maestro, Schrödinger*; LLC: New York, NY, USA, 2019; Available online: <https://www.schrodinger.com/maestro>. (accessed on 13 January 2020).
44. Kálai, T.; Szabó, Z.; Jekő, J.; Hideg, K. Synthesis of New Allylic Nitroxides via the Wadsworth-Emmons Reaction. *Org. Prep. Proced. Int.* **1996**, *28*, 443–452. [[CrossRef](#)]
45. Morris, G.M.; Huey, R.; Lindstrom, W.; Sanner, M.F.; Belew, R.K.; Goodsell, D.S.; Olson, A.J. AutoDock4 and AutoDockTools4: Automated docking with selective receptor flexibility. *J. Comput. Chem.* **2009**, *30*, 2785–2791. [[CrossRef](#)] [[PubMed](#)]
46. Liu, T.; Qian, G.; Wang, W.; Zhang, Y. Molecular docking to understand the metabolic behavior of GNF-351 by CYP3A4 and its potential drug–drug interaction with ketoconazole. *Eur. J. Drug Metab. Pharmacokinet.* **2015**, *40*, 235–238. [[CrossRef](#)]
47. Shahrokh, K.; Orendt, A.; Yost, G.S.; Cheatham, T.E. 3rd Quantum mechanically derived AMBER-compatible heme parameters for various states of the cytochrome P450 catalytic cycle. *J. Comput. Chem.* **2012**, *33*, 119–133. [[CrossRef](#)]

